

## Larger mutual inclinations for the shortest-period planets

FEI DAI,<sup>1,2</sup> KENTO MASUDA,<sup>2,3</sup> AND JOSHUA N. WINN<sup>2</sup>

<sup>1</sup>*Department of Physics and Kavli Institute for Astrophysics and Space Research,  
Massachusetts Institute of Technology, Cambridge, MA, 02139, USA*

<sup>2</sup>*Department of Astrophysical Sciences, Princeton University, 4 Ivy Lane, Princeton, NJ, 08544, USA*

<sup>3</sup>*NASA Sagan Fellow*

(Received ?; Revised ?; Accepted ?)

Submitted to AAS

### ABSTRACT

The *Kepler* mission revealed a population of compact multiple-planet systems with orbital periods shorter than a year, and occasionally even shorter than a day. By analyzing a sample of 102 *Kepler* and *K2* multi-planet systems, we measure the minimum difference  $\Delta I$  between the orbital inclinations, as a function of the orbital distance of the innermost planet. This is accomplished by fitting all the planetary signals simultaneously, constrained by an external estimate of the stellar mean density. We find  $\Delta I$  to be larger when the inner orbit is smaller, a trend that does not appear to be a selection effect. We find that planets with  $a/R_\star < 5$  have a dispersion in  $\Delta I$  of  $6.7 \pm 0.6$  degrees, while planets with  $5 < a/R_\star < 12$  have a dispersion of  $2.0 \pm 0.1$  degrees. The planetary pairs with higher mutual inclinations also tend to have larger period ratios. These trends suggest that the shortest-period planets have experienced both inclination excitation and orbital shrinkage.

*Keywords:* planets and satellites: dynamical evolution and stability, planets and satellites: formation

### 1. INTRODUCTION

One of the revelations of the *Kepler* mission was that Sun-like stars often host planets with sizes between those of Earth and Neptune and orbital periods shorter than a year (Borucki et al. 2011). The formation of these short-period planets and their relationship to wider-orbiting planets are not understood. An interesting clue is that the population of planets with the shortest periods ( $\lesssim 10$  days) is different, in some respects, from the population with longer periods.

One difference is in the planet occurrence rate. The function  $d \log N / d \log P$ , where  $N$  is the mean number of planets per star and  $P$  is the orbital period, increases with period from 0.2–10 days before leveling off to a constant value out to at least 100 days (Petigura et al. 2018). Another difference is that stars hosting sub-Neptune planets with periods shorter than about 10 days tend to have higher metallicities than those hosting planets with longer periods (Mulders et al. 2016; Petigura et al.

2018; Wilson et al. 2018). A third difference is in the period ratios between adjacent planets. When the inner planet’s period is shorter than a few days, the period ratio tends to be larger than when both planets have longer periods (Steffen & Farr 2013).

This *Letter* describes another clue, which we found in the distribution of mutual inclinations. Several scenarios have been proposed to explain the shortest-period planets. In almost all these scenarios, the planet’s orbit is initially wider, because of the theoretical difficulty of building a rocky core in close proximity to the star. Some of the proposed mechanisms to shrink the orbits also involve raising the inclination (Hansen & Murray 2015; Petrovich et al. 2018), while others predict low inclinations (e.g., Lee & Chiang 2017). Previous studies of *Kepler* systems concluded that the mutual inclinations are typically  $\lesssim 5^\circ$ , based on population statistics (Tremaine & Dong 2012; Fabrycky et al. 2014; Fang & Margot 2012). Here, we focus on systems with the closest-orbiting planets, and attempt to measure the mutual inclination of each system directly by fitting the transit light curves.

## 2. SAMPLE SELECTION

Any sample of planets detected with the transit method is strongly biased against systems with large mutual inclinations. However, as the planet’s orbit becomes smaller, the range of transiting inclinations becomes larger. The requirement is  $\cos I < R_\star/a$ , where  $I$  is the inclination,  $R_\star$  is the stellar radius, and  $a$  is the orbital distance. For  $a/R_\star = 4$  (corresponding to  $P \approx 1$  day for a Sun-like star), transits can occur for inclinations between  $75\text{--}90^\circ$ . Therefore, by measuring the inclinations of innermost pair of transiting planets around the same star, we can place a lower bound on the mutual inclination ranging up to  $15^\circ$  for the most favorable cases.

For this study, we selected the *Kepler* multiple-planet systems with apparent *Kepler* magnitude ( $Kp$ ) brighter than 14, for which the innermost planet has a radius smaller than  $4 R_\oplus$ , a transit signal-to-noise ratio (SNR) greater than 20, and  $a/R_\star < 12$ . The limit on  $Kp$  and SNR ensures that the stars have been well characterized and the transit signals can be modeled precisely. The limit on planet size excludes giant planets, which may have a completely different history of formation and evolution than smaller planets. The limit on  $a/R_\star$  corresponds to an allowed range of inclinations of  $85\text{--}90^\circ$ . We augmented our sample with planets with periods  $< 1$  day discovered with *K2* data. We expect the *Kepler* and *K2* systems to be drawn from similar populations, since the observations were made with the same telescope and achieved nearly equivalent photometric precision after correcting for *K2* systematics. Table 1 reports the most important characteristics of the sample.

## 3. CONSTRAINTS ON MEAN STELLAR DENSITY

When fitting a transit light curve, there is often a strong covariance between  $I$  and  $a/R_\star$ . To reduce this covariance, we enforced an external constraint on the stellar mean density  $\rho_\star$ , which is related to  $a/R_\star$  through Kepler’s third law. The external constraint came from fitting stellar-evolutionary models to the observed spectroscopic parameters,  $K$ -band apparent magnitude, and parallax. We used spectroscopic parameters from the California-*Kepler* survey (Petigura et al. 2017) whenever available, and from other sources as needed (see Table 1). We imposed a minimum uncertainty of 100 K in the effective temperature to account for possible systematic errors. The  $K$  magnitudes were from the Two Micron All Sky Survey (2MASS; Skrutskie et al. 2006), after correcting for extinction using  $A_K = 0.443 E(B - V)$  with the value of  $E(B - V)$  from Bovy et al. (2016) (and adopting a 30% uncertainty). The parallaxes were from the *Gaia* Data Release 2 (Gaia Collaboration et al.

2018), although in practice we used the distance estimates provided by Bailer-Jones et al. (2018). The stellar-evolutionary models were from the Dartmouth Stellar Evolution Database (Dotter et al. 2008) and were compared to the data using the `isochrones` package by Morton (2015). The results are given in Column 2 of Table 1. The typical uncertainty is 8%.

As a consistency check, we compared the isochrone-based mean densities with those that were derived from asteroseismology by Van Eylen & Albrecht (2015). On average, the isochrone densities are 5% smaller than the asteroseismic densities, with a dispersion of 5%. This suggests that one or both methods are subject to systematic errors of a few percent. This level of error does not have an appreciable effect on the subsequent results, as we verified directly, by repeating the analysis using the asteroseismic densities in place of the isochrone-based densities whenever both were available.

## 4. LIGHT-CURVE ANALYSIS

For the *Kepler* systems we used the Pre-search Data Conditioning light curves, and for the *K2* systems we used the target pixel files, both were obtained from the Mikulski Archive for Space Telescopes<sup>1</sup>. To construct the *K2* time series and mitigate the systematics from the rolling motion of the spacecraft, we used the code described by Dai et al. (2017). Prior to transit modeling, we removed any long-term photometric trends due to stellar variability or instrumental effects. We masked out the known transits, and fitted the transit-free light curve with a cubic spline of width 0.75 days. In cases for which a nearby stellar companion was reported by Furlan et al. (2017), we corrected the light curve for the “diluting” effect of the companion.

For each transit, we isolated the segment of data spanning three times the transit duration, centered on the midpoint. We visually inspected each transit and removed those few that were obviously damaged by systematic effects. We used the `Batman` code for transit modeling (Kreidberg 2015). The free parameters were the orbital period  $P$ , the midtransit time ( $T_c$ ), the planet-to-star radius ratio ( $R_p/R_\star$ ), the scaled orbital distance ( $a/R_\star$ ), and  $\cos I$ . We adopted a quadratic limb darkening profile, with coefficients subject to Gaussian priors with widths of 0.3 and mean values determined with EXOFAST<sup>2</sup> (Eastman et al. 2013). For the long-cadence data, we computed the model light curve at 1-minute intervals and averaged it to 30 minutes before comparing it to the data.

<sup>1</sup> <https://archive.stsci.edu>

<sup>2</sup> [astroutils.astronomy.ohio-state.edu/exofast/limbdark.shtml](http://astroutils.astronomy.ohio-state.edu/exofast/limbdark.shtml).

To account for possible transit-timing variations, we used an iterative process. First, a constant-period transit model was optimized based on all the data. Next, this model was used as a template to derive individual transit times, by refitting each transit with the free parameters limited to the midtransit time and a quadratic function of time to account for stellar variability. Then, we fitted a linear function of epoch to the transit times, to see if this fit was satisfactory, or if a sinusoidal model provided a better description. We combined all the data to create a phase-folded light curve, where the folding was based on either a constant period, or the individually measured transit times if TTVs had been detected. This phase-folded light curve was then fitted, leading to an improved template for measuring individual transit times. This process converged after 2-3 iterations. We did not end up identifying any TTVs that had not already been flagged by [Ofir et al. \(2018\)](#).

Finally, we fitted the phase-folded light curves for all the planets in each system simultaneously, while imposing an external constraint on the stellar mean density (Section 3). This was done with the Markov Chain Monte Carlo method as implemented by [Foreman-Mackey et al. \(2013\)](#). We imposed a Jeffreys prior on  $R_p/R_*$  and a uniform prior on  $\cos I$ . We restricted  $\cos I > 0$  because transit data alone cannot be used to determine the sign of  $\cos I$ . We assumed the orbit of the innermost planet to be circular, since tidal circularization is expected to be rapid for  $a/R_* < 12$ . The outer planets were allowed to have eccentric orbits. Uniform priors were adopted for  $\sqrt{e} \cos \omega$  and  $\sqrt{e} \sin \omega$ , where  $e$  is the eccentricity and  $\omega$  is the argument of pericenter.

Table 1 reports the results for  $a/R_*$  and  $I$ . For a visual appreciation of the task of measuring inclinations, Figure 2 shows three representative light curves. Also shown are the residuals between the data and two different models: one in which the inclination is allowed to vary freely, and one in which it is held fixed at  $90^\circ$ .

As a test of robustness, we repeated the entire analysis, allowing eccentric orbits for all planets. Naturally, this broadened the allowed range of inclinations, but led to no qualitative changes in the results. For further validation, we performed inject-and-recovery simulations. We focused on the planets with periods shorter than one day, for which the coarse time sampling is of greatest concern. Beginning with the original time series (prior to any detrending), we injected a transit signal into the data with the parameters of the best-fitting model but a different midtransit time and orbital inclination. The fake signals were subjected to the same procedures as the real signals. This was repeated for 5 choices of  $\cos I$  over the range for which transits occur. Figure 1 com-

pares the injected and recovered inclinations, with error bars based on the 68% credible intervals. The agreement is almost always within  $1\text{-}\sigma$ , lending confidence to the results. Toward  $90^\circ$ , the recovered inclination always falls below the identity line, but this is only because we chose to plot the median of the posterior, which is necessarily lower than  $90^\circ$ .

## 5. MINIMUM MUTUAL INCLINATIONS

For each system, we computed  $\Delta I = |I_1 - I_2|$ , where  $I_1$  and  $I_2$  are the fitted orbital inclinations. In general,  $\Delta I$  is a lower bound on the mutual inclination. It is equal to the mutual inclination only if the two planets' trajectories across the stellar disk are parallel and on the same hemisphere of the star.

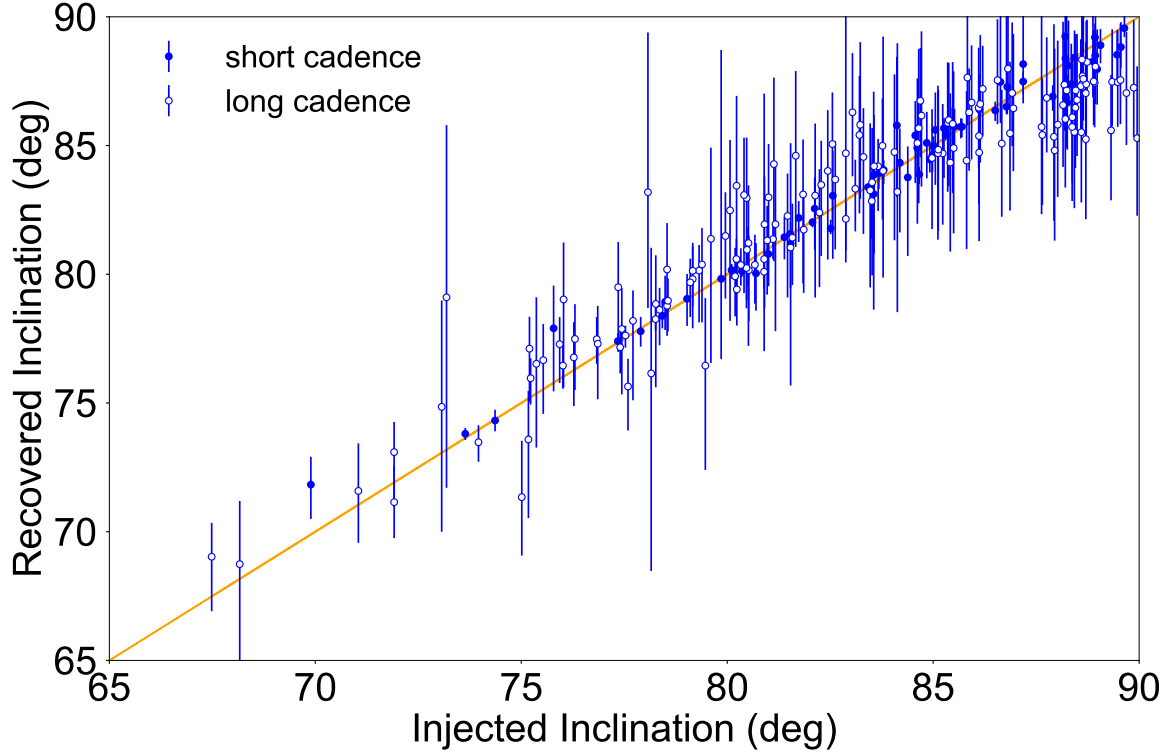
Figure 3 shows  $\Delta I$  as a function of  $a/R_*$  for the innermost planet. Among the systems with the closest-orbiting planets, there are about 10 systems for which  $\Delta I > 5^\circ$ , larger than the typical mutual inclinations that have been inferred for wider-orbiting planets.<sup>3</sup> The planets with  $a/R_* > 5$  almost all have  $\Delta I < 5^\circ$ , even though values of  $5\text{--}10^\circ$  could have been detected in many cases. This is consistent with previous studies of the *Kepler* multi-planet systems, which concluded that the mutual inclinations are likely to be a few degrees or smaller ([Tremaine & Dong 2012](#); [Fabrycky et al. 2014](#); [Fang & Margot 2012](#)). The planets with smaller values of  $a/R_*$  have a broader distribution of  $\Delta I$ , nearly filling the full range of inclinations compatible with transits.

Figure 3 also shows  $\Delta I$  as a function of the period ratio between the innermost two planets. Higher values of  $\Delta I$  are associated with larger period ratios. This reflects a pattern noted by [Steffen & Farr \(2013\)](#): the period ratios tend to be higher when the inner planet's period is shorter than about one day. In that sense, the innermost planets are dynamically more separated. Our results show that these planets are also associated with minimum mutual inclinations ranging up to  $10^\circ$ , higher than that of the broader population of multi-planet systems.

We quantified these impressions with a hierarchical Bayesian analysis. We compared the Bayesian evidence for the following models for the  $\Delta I$  distribution:

1. A Rayleigh distribution, with width  $\sigma$ .
2. A Rayleigh distribution in which the width varies with orbital distance:  $\sigma = \sigma_0 (a/R_*)^m$ .

<sup>3</sup> The relatively large mutual inclination of EPIC 248435473b ( $\Delta I = 12.67^{+0.68}_{-0.75}$  deg) was also noted by [Rodríguez et al. \(2018\)](#).



**Figure 1.** Results of the inject-and-recover test for orbital inclination. Filled circles are for systems observed in short-cadence mode (1-minute sampling) and open circles are for long-cadence mode (30-minute).

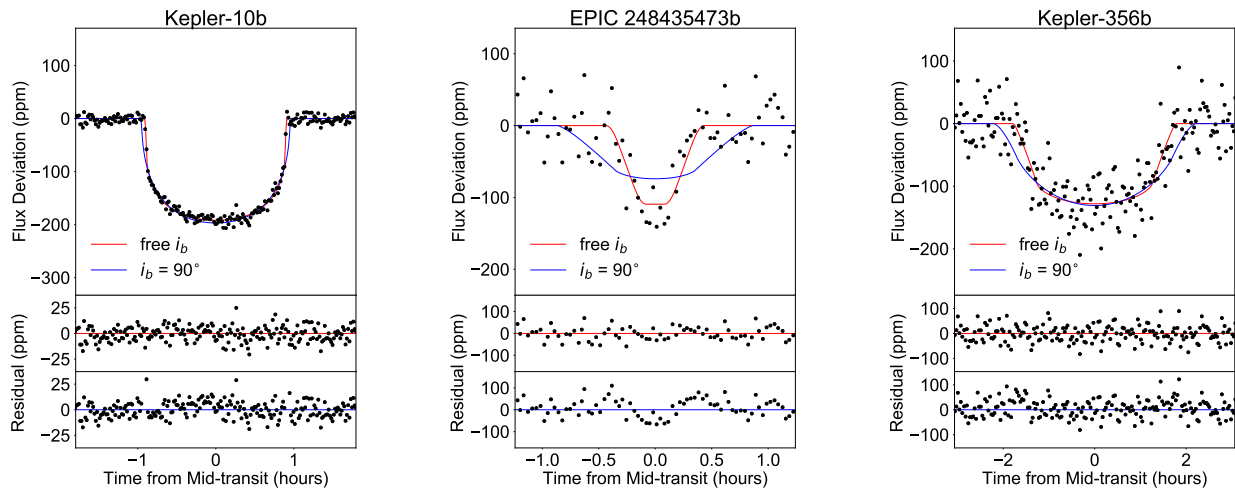


**Figure 2.** Signatures of inclination in the light curves. Shown are three representative phase-folded light curves, along with the best-fitting model (red curve), the best fitting model with  $I = 90^\circ$  (blue curve), and the corresponding residuals. In all these cases, there are patterned residuals in lowest panel, indicating that  $I = 90^\circ$  is disfavored.

3. A Rayleigh distribution in which the width changes abruptly from  $\sigma_{\text{in}}$  to  $\sigma_{\text{out}}$  at a critical value of  $a/R_{\star}$ .
4. A Rayleigh distribution in which the width changes abruptly from  $\sigma_{\text{in}}$  to  $\sigma_{\text{out}}$  at a critical value of the period ratio,  $P_2/P_1$ .

To compute the likelihood as a function of the model parameters, we followed the procedure of [Foreman-Mackey et al. \(2014\)](#), using the approximation

$$p(\text{obs}|\theta) \propto \prod_{k=1}^K \frac{1}{N} \sum_{n=1}^N \frac{p(\Delta I_k^n|\theta)}{p_0(\Delta I_k^n)}, \quad (1)$$

where ‘‘obs’’ represents the data,  $k$  specifies the planetary system,  $n$  specifies random samples from the posterior of  $\Delta I$ , and  $\theta$  is the set of hyperparameters. The function  $p_0$  is the prior probability in our transit modeling (Section 4). Since we adopted uniform and independent priors for  $\cos I_1$  and  $\cos I_2$ , it can be shown that

$$p_0(\Delta I) = \frac{1}{16}(\pi - 2\Delta I) \cos(\Delta I). \quad (2)$$

All the hyperparameters were subject to log-uniform priors, except for the exponent  $m$  in Model 2 for which we used a uniform prior. For each model, we determined the credible intervals for the hyperparameters and the Bayesian evidence  $Z$  using the nested sampling code MULTINEST ([Feroz et al. 2009](#)). Table 2 gives the results. Models 2 and 3 are both favored over Model 1 by  $\Delta \log Z > 26$ , corroborating the visual impression that  $\Delta I$  is larger for smaller orbits. Model 4 is not as successful as Models 2 and 3 but still favored over Model 1 by  $\Delta \log Z > 14$ .

## 6. DISCUSSION

We found that when the innermost planet has  $a/R_{\star} \lesssim 5$  (or  $P = 1.3$  days for a Sun-like star), the minimum mutual inclination is often  $5\text{--}10^\circ$ . This is somewhat higher than the typical value of a few degrees that has been previously estimated for the more general population of *Kepler* systems. We also found  $\Delta I$  to decrease with the orbital separation of the innermost planet. This observation does not appear to be purely a selection effect because for planets with  $a/R_{\star}$  between 5 and 10, we could have detected mutual inclinations larger than  $5^\circ$ , and we did not.

These results may be related to some previously noted trends. [Steffen & Coughlin \(2016\)](#) found that the *Kepler* sample of ‘‘hot Earths’’ without additional transiting companions is larger than what one would obtain by drawing planets randomly from the multiple-transiting

systems. A related observation by [Weiss et al. \(2018\)](#) is that the fraction of *Kepler* systems with multiple transiting planets is lower when the innermost planet has a period shorter than a few days. Our results offer a natural explanation: the shortest-period planets tend to have larger mutual inclinations, and thus, are more likely to be observed to transit even when the wider-orbiting companions do not transit. [Zhu et al. \(2018\)](#) also found evidence for relatively high mutual inclinations in some *Kepler* systems, based on the observed frequencies of multiple transiting planets and TTVs. In their model, the inclination dispersion depends on the total number of planets in the system, ranging from  $0.8^\circ$  in five-planet systems to  $\sim 10^\circ$  for two-planet systems. It would be interesting to try and extend the model of [Zhu et al. \(2018\)](#) to allow the mutual inclination to depend on orbital separation in addition to, or instead of, the total number of planets. [Bovaird & Lineweaver \(2017\)](#) proposed that the inner protoplanetary disk may have a flat (rather than flared) geometry in which case the innermost planets tend to form with larger mutual inclinations.

We emphasize that  $\Delta I$  only represents a lower bound on the mutual inclination. Moreover, if there exist systems with much larger mutual inclinations, they would be unlikely to appear in our sample, because the joint transit probability is low. Despite these limitations, our results indicate that the shortest-period planets have a different orbital architecture, with higher mutual inclinations and larger period ratios. This suggests that whatever processes led to the extremely tight orbits of these planets were also responsible for tilting the orbit to higher inclination.

Several theories have been offered for the formation of very short-period sup-Neptune planets, which differ in their predictions for mutual inclinations. [Lee & Chiang \(2017\)](#) proposed that the magnetospheric truncation radius determines the innermost orbit where planets can form. In this scenario, planets begin with nearly-circular, well-aligned orbits, and the innermost planet undergoes tidal orbital decay. There is no obvious agent for exciting inclinations, and therefore this scenario does not provide an explanation for the larger mutual inclinations of the shortest-period planets. Likewise, the formation scenarios proposed by [Terquem \(2014\)](#) and [Schlaufman et al. \(2010\)](#) do not provide an obvious way to excite inclinations.

[Spalding & Batygin \(2016\)](#) proposed a scenario that does involve inclination excitation. If the host star were initially rotating rapidly, with a non-zero obliquity, the planets’ orbits would undergo nodal precession at different rates and become misaligned, with the innermost

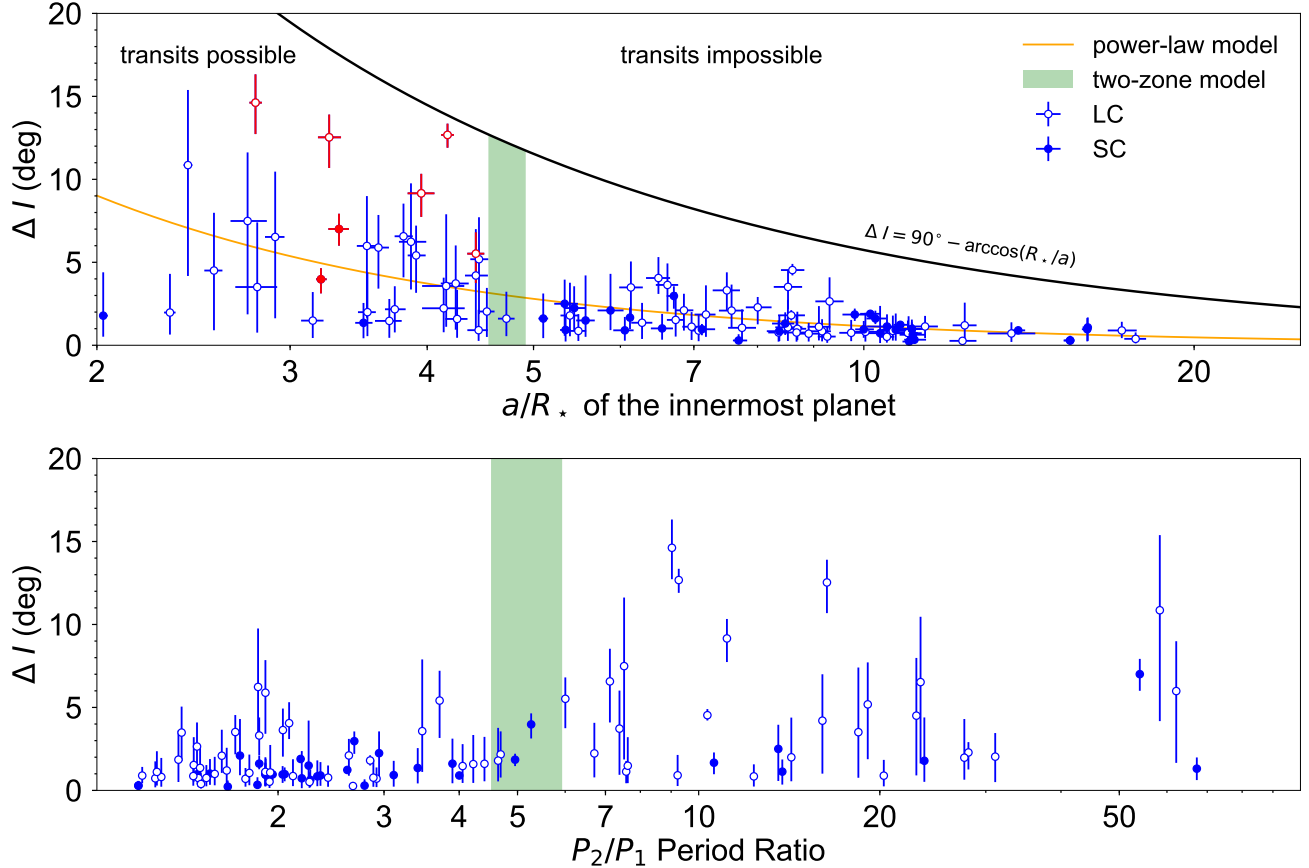


**Figure 3.** Upper Panel: inclination difference  $\Delta I$  versus  $a/R_*$  of the innermost planet. Filled points are for systems observed in short-cadence mode and hollow points are for long-cadence. The black line is the boundary above which the inner planet would not transit, assuming  $i_2 = 90^\circ$ . The orange line represents Model 2. The green zone represents the 68% credible region for the critical value of  $a/R_*$ , in Model 3. Highlighted in red are those data points that are more than 3 standard deviations away from zero: Kepler-10, EPIC 248435473, K2-223, Kepler-312, WASP-47, KOI-2393 and Kepler-653. Lower Panel:  $\Delta I$  versus orbital period ratio  $P_2/P_1$ . The green zone is the 68% credible interval for the critical value of  $P_2/P_1$ , in Model 3.

planet being most strongly affected. The star would only need to be tilted by a few degrees to explain the observed values of  $\Delta I$ . It is not clear whether this scenario would result in an association between higher mutual inclination and larger period ratios, as we have observed.

In the “secular chaos” or “high- $e$  migration” scenario proposed by Petrovich et al. (2018), the innermost planet of a multi-planet system is launched into a high-eccentricity orbit via chaotic secular interactions. If the period is short and the eccentricity becomes high enough ( $\approx 0.8$ ), tidal interactions with the host star shrink the orbit. Since eccentricity and inclination are excited together, this theory predicts that the shortest-period planets should have larger mutual inclinations, in qualitative agreement with our results. A potential problem with this picture is that for systems in mean-motion resonance (MMR), the dynamics may be dominated by the resonance instead of secular interactions. The sample of

USP systems has a decent fraction of systems that are in or near MMR (5 out of 13 systems with at least 2 exterior planets).

Another possibility is forced-eccentricity migration, in which the interaction with outer companions (secular-forcing, or MMR) continually excites the eccentricity of the innermost planet. This allows eccentricity tides to dissipate energy and shrink the orbit (see, e.g., Hansen & Murray 2015). Since the planet’s eccentricity never exceeds a few percent, the inclinations are only excited to a few degrees, perhaps not enough to be compatible with our results.

We thank Vincent Van Eylen, Daniel Fabrycky, Bonan Pu, Songhu Wang, and Cristobal Petrovich for helpful discussions. We are also grateful to the referee for a prompt report.

This work made use of the `gaia-kepler.fun` crossmatch database created by Megan Bedell. Work by F.D. and J.N.W. was supported by the Heising-Simons Foundation. Work by K.M. was performed in part under

contract with the California Institute of Technology (Caltech)/Jet Propulsion Laboratory (JPL) funded by NASA through the Sagan Fellowship Program executed by the NASA Exoplanet Science Institute.

## REFERENCES

- Bailer-Jones, C. A. L., Rybizki, J., Fouesneau, M., Mantelet, G., & Andrae, R. 2018, ArXiv e-prints, arXiv:1804.10121
- Barragán, O., Gandolfi, D., Dai, F., et al. 2018, *A&A*, 612, A95
- Becker, J. C., Vanderburg, A., Adams, F. C., Rappaport, S. A., & Schwengeler, H. M. 2015, *ApJL*, 812, L18
- Borucki, W. J., Koch, D. G., Basri, G., et al. 2011, *ApJ*, 728, 117
- Bovaird, T., & Lineweaver, C. H. 2017, *MNRAS*, 468, 1493
- Bovy, J., Rix, H.-W., Green, G. M., Schlafly, E. F., & Finkbeiner, D. P. 2016, *ApJ*, 818, 130
- Dai, F., Winn, J. N., Yu, L., & Albrecht, S. 2017, *AJ*, 153, 40
- Dotter, A., Chaboyer, B., Jevremović, D., et al. 2008, *ApJS*, 178, 89
- Dressing, C. D., Vanderburg, A., Schlieder, J. E., et al. 2017, *AJ*, 154, 207
- Eastman, J., Gaudi, B. S., & Agol, E. 2013, *PASP*, 125, 83
- Everett, M. E., Howell, S. B., Silva, D. R., & Szkody, P. 2013, *ApJ*, 771, 107
- Fabrycky, D. C., Lissauer, J. J., Ragozzine, D., et al. 2014, *ApJ*, 790, 146
- Fang, J., & Margot, J.-L. 2012, *ApJ*, 761, 92
- Feroz, F., Hobson, M. P., & Bridges, M. 2009, *MNRAS*, 398, 1601
- Foreman-Mackey, D., Hogg, D. W., Lang, D., & Goodman, J. 2013, *PASP*, 125, 306
- Foreman-Mackey, D., Hogg, D. W., & Morton, T. D. 2014, *ApJ*, 795, 64
- Fressin, F., Torres, G., Charbonneau, D., et al. 2013, *ApJ*, 766, 81
- Furlan, E., Ciardi, D. R., Everett, M. E., et al. 2017, *AJ*, 153, 71
- Gaia Collaboration, Brown, A. G. A., Vallenari, A., et al. 2018, ArXiv e-prints, arXiv:1804.09365
- Guenther, E. W., Barragán, O., Dai, F., et al. 2017, *A&A*, 608, A93
- Hansen, B. M. S., & Murray, N. 2015, *MNRAS*, 448, 1044
- Howard, A. W., Marcy, G. W., Bryson, S. T., et al. 2012, *ApJS*, 201, 15
- Kipping, D. M. 2013, *MNRAS*, 435, 2152
- Kreidberg, L. 2015, *PASP*, 127, 1161
- Lee, E. J., & Chiang, E. 2017, *ApJ*, 842, 40
- MacDonald, M. G., Ragozzine, D., Fabrycky, D. C., et al. 2016, *AJ*, 152, 105
- Mann, A. W., Gaidos, E., & Ansdell, M. 2013, *ApJ*, 779, 188
- Mathur, S., Huber, D., Batalha, N. M., et al. 2017, *ApJS*, 229, 30
- Mayo, A. W., Vanderburg, A., Latham, D. W., et al. 2018, *AJ*, 155, 136
- Morton, T. D. 2015, isochrones: Stellar model grid package, Astrophysics Source Code Library, , ascl:1503.010
- Mulders, G. D., Pascucci, I., Apai, D., Frasca, A., & Molenda-Żakowicz, J. 2016, *AJ*, 152, 187
- Ofir, A., Xie, J.-W., Jiang, C.-F., Sari, R., & Aharonson, O. 2018, *ApJS*, 234, 9
- Petigura, E. A., Howard, A. W., Marcy, G. W., et al. 2017, *AJ*, 154, 107
- Petigura, E. A., Marcy, G. W., Winn, J. N., et al. 2018, *AJ*, 155, 89
- Petrovich, C., Deibert, E., & Wu, Y. 2018, ArXiv e-prints, arXiv:1804.05065
- Rodriguez, J. E., Becker, J. C., Eastman, J. D., et al. 2018, ArXiv e-prints, arXiv:1806.08368
- Sanchis-Ojeda, R., Rappaport, S., Winn, J. N., et al. 2014, *ApJ*, 787, 47
- Santerne, A., Brugger, B., Armstrong, D. J., et al. 2018, *Nature Astronomy*, 2, 393
- Schlaufman, K. C., Lin, D. N. C., & Ida, S. 2010, *ApJL*, 724, L53
- Skrutskie, M. F., Cutri, R. M., Stiening, R., et al. 2006, *AJ*, 131, 1163
- Spalding, C., & Batygin, K. 2014, *ApJ*, 790, 42
- . 2016, *ApJ*, 830, 5
- Steffen, J. H., & Coughlin, J. L. 2016, Proceedings of the National Academy of Science, 113, 12023
- Steffen, J. H., & Farr, W. M. 2013, *ApJL*, 774, L12
- Terquem, C. 2014, *MNRAS*, 444, 1738
- Tremaine, S., & Dong, S. 2012, *AJ*, 143, 94
- Van Eylen, V., & Albrecht, S. 2015, *ApJ*, 808, 126
- Vanderburg, A., Bieryla, A., Duvet, D. A., et al. 2016, *ApJL*, 829, L9
- Weiss, L. M., Isaacson, H. T., Marcy, G. W., et al. 2018, ArXiv e-prints, arXiv:1808.03010

Wilson, R. F., Teske, J., Majewski, S. R., et al. 2018, AJ,  
155, 68

Wittenmyer, R. A., Sharma, S., Stello, D., et al. 2018, AJ,  
155, 84  
Zhu, W., Petrovich, C., Wu, Y., Dong, S., & Xie, J. 2018,  
ApJ, 860, 101



Table 1. Transit Modeling Results

Planet	$\rho_*$ (g cm <sup>-3</sup> )	Source	$P_1$ (days)	$P_2/P_1$	$a/R_*$	$i$ (°)	$\Delta I$ (°)	Cadence	TTV
KOI-1843.03	5.115 <sup>+0.155</sup> <sub>-0.117</sub>	Mann et al. (2013)+Gaia	0.177	23.72	2.03 <sup>+0.02</sup> <sub>-0.02</sub>	87.17 <sup>+2.10</sup> <sub>-2.86</sub>	1.71 <sup>+2.91</sup> <sub>-1.22</sub>	SC	
EPIC-211305568b	6.868 <sup>+0.214</sup> <sub>-0.186</sub>	Dressing et al. (2017)+Gaia	0.198	58.39	2.42 <sup>+0.02</sup> <sub>-0.02</sub>	77.71 <sup>+7.35</sup> <sub>-5.05</sub>	10.19 <sup>+5.16</sup> <sub>-7.18</sub>	LC	
K2-141b	3.089 <sup>+0.130</sup> <sub>-0.110</sub>	Barragán et al. (2018)+Gaia	0.280	27.63	2.33 <sup>+0.03</sup> <sub>-0.03</sub>	86.81 <sup>+2.34</sup> <sub>-3.41</sub>	2.08 <sup>+2.17</sup> <sub>-1.42</sub>	LC	
Kepler-42c	56.740 <sup>+15.410</sup> <sub>-15.410</sub>	Mann et al. (2013)+Gaia	0.453	2.68	6.71 <sup>+0.05</sup> <sub>-0.11</sub>	89.14 <sup>+0.63</sup> <sub>-0.91</sub>	2.95 <sup>+0.60</sup> <sub>-0.77</sub>	SC	
K2-183b	1.452 <sup>+0.100</sup> <sub>-0.087</sub>	Mayo et al. (2018)	0.469	23.00	2.55 <sup>+0.05</sup> <sub>-0.05</sub>	85.11 <sup>+3.25</sup> <sub>-4.03</sub>	4.19 <sup>+3.93</sup> <sub>-3.27</sub>	LC	
K2-223b	1.611 <sup>+0.061</sup> <sub>-0.072</sub>	Mayo et al. (2018)	0.506	9.03	2.79 <sup>+0.04</sup> <sub>-0.04</sub>	73.80 <sup>+1.93</sup> <sub>-1.15</sub>	14.72 <sup>+1.50</sup> <sub>-2.11</sub>	LC	
Kepler-990c	1.460 <sup>+0.409</sup> <sub>-0.343</sub>	CKS+Gaia	0.538	18.42	2.79 <sup>+0.12</sup> <sub>-0.13</sub>	84.86 <sup>+3.67</sup> <sub>-3.74</sub>	3.82 <sup>+3.89</sup> <sub>-2.96</sub>	LC	
K2-106b	1.426 <sup>+0.094</sup> <sub>-0.086</sub>	Guenther et al. (2017)+Gaia	0.571	23.38	2.91 <sup>+0.06</sup> <sub>-0.06</sub>	82.65 <sup>+5.03</sup> <sub>-3.94</sub>	6.31 <sup>+4.02</sup> <sub>-4.82</sub>	LC	
K2-229b	2.451 <sup>+0.149</sup> <sub>-0.147</sub>	Santerne et al. (2018)+Gaia	0.584	14.25	3.53 <sup>+0.06</sup> <sub>-0.07</sub>	87.01 <sup>+2.14</sup> <sub>-2.54</sub>	1.84 <sup>+2.26</sup> <sub>-1.28</sub>	LC	
KOI-787.03	1.104 <sup>+0.154</sup> <sub>-0.140</sub>	Everett et al. (2013)+Gaia	0.589	7.52	2.75 <sup>+0.10</sup> <sub>-0.11</sub>	80.86 <sup>+5.82</sup> <sub>-3.99</sub>	7.55 <sup>+4.07</sup> <sub>-5.61</sub>	LC	
KOI-2250.02	2.506 <sup>+0.155</sup> <sub>-0.178</sub>	CKS+Gaia	0.626	4.69	3.74 <sup>+0.08</sup> <sub>-0.08</sub>	84.51 <sup>+3.14</sup> <sub>-2.30</sub>	2.27 <sup>+1.46</sup> <sub>-1.49</sub>	LC	
Kepler-607b	2.047 <sup>+0.152</sup> <sub>-0.108</sub>	CKS+Gaia	0.638	62.18	3.53 <sup>+0.07</sup> <sub>-0.07</sub>	83.68 <sup>+3.98</sup> <sub>-3.09</sub>	5.89 <sup>+3.06</sup> <sub>-3.96</sub>	LC	
EPIC-248435473b	3.166 <sup>+0.143</sup> <sub>-0.105</sub>	Rodriguez et al. (2018)+Gaia	0.658	9.27	4.17 <sup>+0.05</sup> <sub>-0.05</sub>	76.40 <sup>+1.93</sup> <sub>-0.27</sub>	12.67 <sup>+0.68</sup> <sub>-0.75</sub>	LC	d, e
Kepler-1340b	1.421 <sup>+0.116</sup> <sub>-0.134</sub>	CKS+Gaia	0.665	7.62	3.14 <sup>+0.08</sup> <sub>-0.07</sub>	87.62 <sup>+1.73</sup> <sub>-2.26</sub>	1.47 <sup>+1.60</sup> <sub>-1.07</sub>	LC	
KOI-191.03	1.535 <sup>+0.179</sup> <sub>-0.142</sub>	CKS+Gaia	0.709	3.41	3.49 <sup>+0.07</sup> <sub>-0.07</sub>	85.73 <sup>+2.09</sup> <sub>-1.41</sub>	1.39 <sup>+1.13</sup> <sub>-0.90</sub>	SC	
Kepler-32f	4.577 <sup>+0.164</sup> <sub>-0.130</sub>	Mann et al. (2013)+Gaia	0.743	3.90	5.11 <sup>+0.05</sup> <sub>-0.05</sub>	87.68 <sup>+1.38</sup> <sub>-1.46</sub>	1.64 <sup>+1.33</sup> <sub>-1.16</sub>	SC	b, c, e
KOI-2248.03	2.343 <sup>+0.365</sup> <sub>-0.352</sub>	Everett et al. (2013)+Gaia	0.762	3.47	4.15 <sup>+0.16</sup> <sub>-0.19</sub>	85.58 <sup>+2.85</sup> <sub>-2.42</sub>	3.39 <sup>+4.45</sup> <sub>-2.32</sub>	LC	
Kepler-1067b	1.792 <sup>+0.098</sup> <sub>-0.127</sub>	CKS+Gaia	0.762	7.12	3.80 <sup>+0.09</sup> <sub>-0.07</sub>	81.58 <sup>+2.69</sup> <sub>-1.73</sub>	6.75 <sup>+1.67</sup> <sub>-2.60</sub>	LC	
KOI-1360.03	2.879 <sup>+0.131</sup> <sub>-0.183</sub>	CKS+Gaia	0.764	19.09	4.46 <sup>+0.08</sup> <sub>-0.07</sub>	83.83 <sup>+3.35</sup> <sub>-2.34</sub>	5.23 <sup>+2.37</sup> <sub>-3.28</sub>	LC	
KOI-2393.02	2.809 <sup>+0.148</sup> <sub>-0.169</sub>	CKS+Gaia	0.767	6.00	4.44 <sup>+0.08</sup> <sub>-0.08</sub>	83.34 <sup>+1.76</sup> <sub>-1.11</sub>	5.59 <sup>+1.30</sup> <sub>-1.86</sub>	LC	
K2-187b	1.889 <sup>+0.113</sup> <sub>-0.123</sub>	Mayo et al. (2018)	0.774	3.71	3.91 <sup>+0.08</sup> <sub>-0.08</sub>	82.61 <sup>+2.48</sup> <sub>-1.55</sub>	5.42 <sup>+1.78</sup> <sub>-2.60</sub>	LC	
KOI-1239.01	1.628 <sup>+0.183</sup> <sub>-0.196</sub>	CKS+Gaia	0.783	4.05	3.70 <sup>+0.09</sup> <sub>-0.11</sub>	87.68 <sup>+1.69</sup> <sub>-2.18</sub>	1.42 <sup>+1.36</sup> <sub>-0.98</sub>	LC	
WASP-47e	0.980 <sup>+0.083</sup> <sub>-0.079</sub>	Becker et al. (2015)+Gaia	0.790	5.27	3.20 <sup>+0.04</sup> <sub>-0.03</sub>	84.76 <sup>+0.98</sup> <sub>-0.78</sub>	4.00 <sup>+0.64</sup> <sub>-0.84</sub>	SC	b, c
Kepler-10b	1.068 <sup>+0.001</sup> <sub>-0.007</sub>	Astreoseismology	0.837	54.08	3.406 <sup>+0.005</sup> <sub>-0.005</sub>	84.02 <sup>+0.12</sup> <sub>-0.11</sub>	5.82 <sup>+0.16</sup> <sub>-0.17</sub>	SC	c
Kepler-10b	1.010 <sup>+0.077</sup> <sub>-0.063</sub>	CKS+Gaia	0.838	54.08	3.32 <sup>+0.07</sup> <sub>-0.06</sub>	82.78 <sup>+1.03</sup> <sub>-0.85</sub>	7.03 <sup>+0.84</sup> <sub>-1.02</sub>	SC	c
KOI-1499.02	2.060 <sup>+0.179</sup> <sub>-0.185</sub>	KIC <sup>5</sup> +Gaia	0.841	7.39	4.25 <sup>+0.12</sup> <sub>-0.13</sub>	84.70 <sup>+2.95</sup> <sub>-2.25</sub>	3.91 <sup>+2.33</sup> <sub>-2.69</sub>	LC	
Kepler-732c	5.421 <sup>+0.150</sup> <sub>-0.122</sub>	Mann et al. (2013)+Gaia	0.893	10.60	6.12 <sup>+0.05</sup> <sub>-0.05</sub>	87.92 <sup>+0.64</sup> <sub>-0.48</sub>	1.71 <sup>+0.55</sup> <sub>-0.67</sub>	SC	
Kepler-653c	0.807 <sup>+0.062</sup> <sub>-0.059</sub>	CKS+Gaia	0.900	16.34	3.26 <sup>+0.08</sup> <sub>-0.07</sub>	75.99 <sup>+1.68</sup> <sub>-1.16</sub>	12.38 <sup>+1.52</sup> <sub>-1.72</sub>	LC	
EPIC-206024342b	1.994 <sup>+0.131</sup> <sub>-0.167</sub>	Wittenmyer et al. (2018)+Gaia	0.912	16.06	4.42 <sup>+0.11</sup> <sub>-0.10</sub>	84.60 <sup>+3.62</sup> <sub>-3.16</sub>	3.95 <sup>+3.05</sup> <sub>-3.06</sub>	LC	
HD-3167b	1.916 <sup>+0.114</sup> <sub>-0.107</sub>	Vanderburg et al. (2016)+Gaia	0.960	31.10	4.53 <sup>+0.08</sup> <sub>-0.08</sub>	87.38 <sup>+1.69</sup> <sub>-1.50</sub>	2.04 <sup>+1.46</sup> <sub>-1.54</sub>	LC	
Kepler-1322b	1.437 <sup>+0.228</sup> <sub>-0.240</sub>	KIC+Gaia	0.963	6.71	4.15 <sup>+0.19</sup> <sub>-0.19</sub>	85.59 <sup>+2.60</sup> <sub>-2.35</sub>	2.10 <sup>+1.89</sup> <sub>-1.50</sub>	LC	
KOI-3145.02	3.129 <sup>+0.189</sup> <sub>-0.183</sub>	KIC+Gaia	0.977	4.64	5.41 <sup>+0.12</sup> <sub>-0.10</sub>	86.64 <sup>+2.23</sup> <sub>-2.24</sub>	1.80 <sup>+2.12</sup> <sub>-1.21</sub>	LC	
Kepler-80f	3.026 <sup>+0.107</sup> <sub>-0.136</sub>	CKS+Gaia	0.987	3.11	5.35 <sup>+0.05</sup> <sub>-0.06</sub>	88.85 <sup>+0.89</sup> <sub>-1.00</sub>	0.89 <sup>+0.90</sup> <sub>-0.65</sub>	SC	b, c
Kepler-755b	2.031 <sup>+0.149</sup> <sub>-0.096</sub>	CKS+Gaia	1.269	2.25	5.57 <sup>+0.11</sup> <sub>-0.11</sub>	84.12 <sup>+0.41</sup> <sub>-0.36</sub>	1.58 <sup>+2.67</sup> <sub>-1.07</sub>	SC	
Kepler-198d	1.695 <sup>+0.146</sup> <sub>-0.145</sub>	KIC+Gaia	1.312	13.56	5.34 <sup>+0.16</sup> <sub>-0.12</sub>	87.15 <sup>+2.04</sup> <sub>-1.45</sub>	2.43 <sup>+1.41</sup> <sub>-1.91</sub>	SC	
Kepler-207b	0.334 <sup>+0.027</sup> <sub>-0.025</sub>	CKS+Gaia	1.612	1.91	3.60 <sup>+0.10</sup> <sub>-0.10</sub>	81.77 <sup>+1.55</sup> <sub>-1.23</sub>	5.93 <sup>+1.91</sup> <sub>-2.33</sub>	LC	
Kepler-342e	0.661 <sup>+0.056</sup> <sub>-0.054</sub>	CKS+Gaia	1.644	9.23	4.46 <sup>+0.09</sup> <sub>-0.11</sub>	88.67 <sup>+1.00</sup> <sub>-1.51</sub>	0.85 <sup>+1.19</sup> <sub>-0.58</sub>	LC	c, d
Kepler-322b	2.222 <sup>+0.119</sup> <sub>-0.151</sub>	CKS+Gaia	1.654	2.62	6.86 <sup>+0.13</sup> <sub>-0.14</sub>	86.85 <sup>+1.32</sup> <sub>-0.84</sub>	2.12 <sup>+0.92</sup> <sub>-1.21</sub>	LC	
Kepler-323b	1.135 <sup>+0.109</sup> <sub>-0.102</sub>	KIC+Gaia	1.678	2.12	5.49 <sup>+0.08</sup> <sub>-0.12</sub>	88.51 <sup>+1.01</sup> <sub>-1.37</sub>	0.82 <sup>+1.01</sup> <sub>-0.55</sub>	LC	
Kepler-969c	2.375 <sup>+0.113</sup> <sub>-0.146</sub>	CKS+Gaia	1.683	20.31	7.08 <sup>+0.11</sup> <sub>-0.11</sub>	88.68 <sup>+0.88</sup> <sub>-0.96</sub>	0.82 <sup>+0.96</sup> <sub>-0.60</sub>	LC	
Kepler-1047c	0.371 <sup>+0.037</sup> <sub>-0.030</sub>	CKS+Gaia	1.721	1.85	3.87 <sup>+0.12</sup> <sub>-0.10</sub>	78.25 <sup>+1.78</sup> <sub>-1.20</sub>	6.30 <sup>+3.55</sup> <sub>-2.84</sub>	LC	
Kepler-312b	0.371 <sup>+0.031</sup> <sub>-0.030</sub>	CKS+Gaia	1.772	11.14	3.95 <sup>+0.11</sup> <sub>-0.10</sub>	79.32 <sup>+0.62</sup> <sub>-0.64</sub>	9.12 <sup>+1.19</sup> <sub>-1.38</sub>	LC	c
Kepler-524c	0.410 <sup>+0.037</sup> <sub>-0.031</sub>	CKS+Gaia	1.889	4.22	4.26 <sup>+0.10</sup> <sub>-0.10</sub>	87.24 <sup>+1.91</sup> <sub>-1.97</sub>	1.65 <sup>+1.82</sup> <sub>-1.16</sub>	LC	b
Kepler-1371c	1.440 <sup>+0.086</sup> <sub>-0.066</sub>	CKS+Gaia	2.005	1.45	6.73 <sup>+0.11</sup> <sub>-0.12</sub>	85.91 <sup>+2.20</sup> <sub>-1.08</sub>	1.59 <sup>+1.65</sup> <sub>-1.08</sub>	LC	
Kepler-142b	1.012 <sup>+0.087</sup> <sub>-0.074</sub>	CKS+Gaia	2.024	2.35	6.06 <sup>+0.10</sup> <sub>-0.15</sub>	88.02 <sup>+1.21</sup> <sub>-1.02</sub>	0.89 <sup>+0.81</sup> <sub>-0.62</sub>	SC	
Kepler-326b	1.068 <sup>+0.073</sup> <sub>-0.078</sub>	CKS+Gaia	2.248	2.04	6.62 <sup>+0.16</sup> <sub>-0.15</sub>	84.59 <sup>+0.90</sup> <sub>-0.83</sub>	3.59 <sup>+1.36</sup> <sub>-1.51</sub>	LC	
Kepler-406b	1.133 <sup>+0.105</sup> <sub>-0.090</sub>	CKS+Gaia	2.426	1.91	6.97 <sup>+0.13</sup> <sub>-0.15</sub>	89.07 <sup>+0.62</sup> <sub>-0.92</sub>	1.02 <sup>+0.97</sup> <sub>-0.77</sub>	LC	

Table 1 continued

<sup>5</sup> Mathur et al. (2017)

Table 1 (continued)

Planet	$\rho_*$ (g cm <sup>-3</sup> )	Source	$P_1$ (days)	$P_2/P_1$	$a/R_*$	$i(^{\circ})$	$\Delta I(^{\circ})$	Cadence	TTV
Kepler-314b	1.845 <sup>+0.137</sup> <sub>-0.134</sub>	CKS+Gaia	2.461	2.42	8.35 <sup>+0.19</sup> <sub>-0.18</sub>	88.65 <sup>+0.88</sup> <sub>-1.05</sub>	0.79 <sup>+0.73</sup> <sub>-0.52</sub>	LC	
Kepler-213b	1.110 <sup>+0.098</sup> <sub>-0.096</sub>	CKS+Gaia	2.462	1.96	7.10 <sup>+0.22</sup> <sub>-0.18</sub>	83.99 <sup>+0.37</sup> <sub>-0.32</sub>	0.94 <sup>+0.37</sup> <sub>-0.37</sub>	SC	
Kepler-1311c	0.298 <sup>+0.022</sup> <sub>-0.018</sub>	CKS+Gaia	2.536	4.41	4.72 <sup>+0.08</sup> <sub>-0.08</sub>	87.22 <sup>+1.65</sup> <sub>-1.47</sub>	1.53 <sup>+1.60</sup> <sub>-1.03</sub>	LC	
Kepler-1398b	0.611 <sup>+0.048</sup> <sub>-0.044</sub>	CKS+Gaia	2.788	1.48	6.27 <sup>+0.13</sup> <sub>-0.15</sub>	88.45 <sup>+1.03</sup> <sub>-1.22</sub>	1.45 <sup>+1.29</sup> <sub>-0.98</sub>	LC	
Kepler-221b	2.417 <sup>+0.132</sup> <sub>-0.159</sub>	CKS+Gaia	2.796	2.04	10.00 <sup>+0.22</sup> <sub>-0.19</sub>	88.18 <sup>+0.51</sup> <sub>-0.32</sub>	0.98 <sup>+0.51</sup> <sub>-0.51</sub>	SC	e
Kepler-1542c	0.837 <sup>+0.067</sup> <sub>-0.051</sub>	CKS+Gaia	2.892	1.37	7.18 <sup>+0.15</sup> <sub>-0.15</sub>	85.49 <sup>+0.72</sup> <sub>-0.52</sub>	1.77 <sup>+1.88</sup> <sub>-1.34</sub>	LC	
Kepler-411b	2.630 <sup>+0.132</sup> <sub>-0.139</sub>	CKS+Gaia	3.005	2.61	10.78 <sup>+0.17</sup> <sub>-0.13</sub>	87.71 <sup>+0.19</sup> <sub>-0.16</sub>	1.23 <sup>+0.14</sup> <sub>-0.15</sub>	SC	c
Kepler-1271b	0.951 <sup>+0.105</sup> <sub>-0.090</sub>	KIC+Gaia	3.026	1.79	7.74 <sup>+0.24</sup> <sub>-0.23</sub>	88.10 <sup>+1.22</sup> <sub>-1.03</sub>	1.04 <sup>+1.10</sup> <sub>-0.72</sub>	LC	
Kepler-141b	2.311 <sup>+0.153</sup> <sub>-0.106</sub>	CKS+Gaia	3.108	2.26	10.49 <sup>+0.17</sup> <sub>-0.18</sub>	89.24 <sup>+0.50</sup> <sub>-0.70</sub>	0.52 <sup>+0.53</sup> <sub>-0.36</sub>	LC	
Kepler-203b	1.167 <sup>+0.120</sup> <sub>-0.107</sub>	CKS+Gaia	3.163	1.70	8.53 <sup>+0.24</sup> <sub>-0.25</sub>	84.92 <sup>+0.28</sup> <sub>-0.28</sub>	3.39 <sup>+1.18</sup> <sub>-1.30</sub>	LC	
Kepler-107b	0.581 <sup>+0.049</sup> <sub>-0.049</sub>	Astroseismology	3.180	1.54	6.71 <sup>+0.06</sup> <sub>-0.11</sub>	88.97 <sup>+0.65</sup> <sub>-0.86</sub>	1.62 <sup>+0.80</sup> <sub>-0.94</sub>	SC	
Kepler-107b	0.519 <sup>+0.038</sup> <sub>-0.045</sub>	CKS+Gaia	3.180	1.54	6.54 <sup>+0.15</sup> <sub>-0.14</sub>	87.74 <sup>+1.09</sup> <sub>-0.69</sub>	0.99 <sup>+0.89</sup> <sub>-0.66</sub>	SC	
Kepler-140b	0.904 <sup>+0.080</sup> <sub>-0.067</sub>	CKS+Gaia	3.254	28.07	8.01 <sup>+0.23</sup> <sub>-0.20</sub>	87.45 <sup>+1.08</sup> <sub>-0.55</sub>	2.31 <sup>+0.57</sup> <sub>-1.06</sub>	LC	
Kepler-337b	0.278 <sup>+0.023</sup> <sub>-0.019</sub>	CKS+Gaia	3.293	2.94	5.45 <sup>+0.13</sup> <sub>-0.12</sub>	86.51 <sup>+1.57</sup> <sub>-0.87</sub>	2.16 <sup>+1.27</sup> <sub>-1.31</sub>	SC	
Kepler-111b	1.002 <sup>+0.085</sup> <sub>-0.078</sub>	CKS+Gaia	3.342	67.26	8.48 <sup>+0.18</sup> <sub>-0.22</sub>	88.40 <sup>+0.77</sup> <sub>-0.67</sub>	1.32 <sup>+0.65</sup> <sub>-0.75</sub>	SC	
Kepler-101b	0.311 <sup>+0.027</sup> <sub>-0.022</sub>	CKS+Gaia	3.488	1.73	5.87 <sup>+0.17</sup> <sub>-0.15</sub>	84.22 <sup>+0.73</sup> <sub>-0.46</sub>	2.19 <sup>+2.23</sup> <sub>-1.31</sub>	SC	b
Kepler-18b	1.612 <sup>+0.143</sup> <sub>-0.130</sub>	CKS+Gaia	3.505	2.18	10.14 <sup>+0.24</sup> <sub>-0.20</sub>	86.32 <sup>+0.21</sup> <sub>-0.19</sub>	1.89 <sup>+0.12</sup> <sub>-0.14</sub>	SC	c, d
Kepler-363b	0.396 <sup>+0.034</sup> <sub>-0.033</sub>	CKS+Gaia	3.615	2.09	6.49 <sup>+0.17</sup> <sub>-0.18</sub>	84.02 <sup>+0.64</sup> <sub>-0.54</sub>	4.09 <sup>+1.36</sup> <sub>-1.06</sub>	LC	
Kepler-218b	1.116 <sup>+0.095</sup> <sub>-0.072</sub>	CKS+Gaia	3.619	12.35	9.16 <sup>+0.19</sup> <sub>-0.19</sub>	88.77 <sup>+0.86</sup> <sub>-0.81</sub>	0.80 <sup>+0.81</sup> <sub>-0.58</sub>	LC	
Kepler-20b	1.756 <sup>+0.155</sup> <sub>-0.132</sub>	CKS+Gaia	3.696	1.65	11.00 <sup>+0.15</sup> <sub>-0.17</sub>	88.19 <sup>+0.23</sup> <sub>-0.22</sub>	0.20 <sup>+0.35</sup> <sub>-0.16</sub>	SC	b, c
Kepler-466c	1.505 <sup>+0.241</sup> <sub>-0.259</sub>	CKS+Gaia	3.709	13.77	10.50 <sup>+0.32</sup> <sub>-0.37</sub>	88.76 <sup>+0.79</sup> <sub>-0.78</sub>	1.02 <sup>+0.81</sup> <sub>-0.71</sub>	SC	
Kepler-89b	0.596 <sup>+0.055</sup> <sub>-0.047</sub>	CKS+Gaia	3.743	2.78	7.70 <sup>+0.13</sup> <sub>-0.10</sub>	88.09 <sup>+0.62</sup> <sub>-0.39</sub>	0.28 <sup>+0.38</sup> <sub>-0.18</sub>	SC	c, d, e
Kepler-217d	0.289 <sup>+0.023</sup> <sub>-0.023</sub>	CKS+Gaia	3.887	1.38	6.13 <sup>+0.16</sup> <sub>-0.16</sub>	84.18 <sup>+0.64</sup> <sub>-0.52</sub>	3.53 <sup>+1.52</sup> <sub>-1.86</sub>	LC	
Kepler-380b	0.757 <sup>+0.074</sup> <sub>-0.060</sub>	CKS+Gaia	3.931	1.94	8.54 <sup>+0.24</sup> <sub>-0.24</sub>	86.31 <sup>+0.80</sup> <sub>-0.53</sub>	1.10 <sup>+1.54</sup> <sub>-0.78</sub>	LC	
Kepler-402b	1.068 <sup>+0.099</sup> <sub>-0.092</sub>	CKS+Gaia	4.029	1.52	9.74 <sup>+0.29</sup> <sub>-0.26</sub>	88.06 <sup>+1.03</sup> <sub>-0.67</sub>	0.77 <sup>+0.74</sup> <sub>-0.50</sub>	LC	
Kepler-202b	3.014 <sup>+0.115</sup> <sub>-0.146</sub>	CKS+Gaia	4.069	4.00	13.82 <sup>+0.20</sup> <sub>-0.20</sub>	88.06 <sup>+0.16</sup> <sub>-0.14</sub>	0.91 <sup>+0.16</sup> <sub>-0.14</sub>	SC	
Kepler-625c	0.457 <sup>+0.047</sup> <sub>-0.035</sub>	KIC+Gaia	4.165	1.86	7.49 <sup>+0.23</sup> <sub>-0.21</sub>	85.06 <sup>+0.36</sup> <sub>-0.37</sub>	3.34 <sup>+1.08</sup> <sub>-1.25</sub>	LC	
Kepler-208b	0.745 <sup>+0.068</sup> <sub>-0.060</sub>	CKS+Gaia	4.229	1.77	8.90 <sup>+0.26</sup> <sub>-0.22</sub>	87.30 <sup>+0.87</sup> <sub>-0.50</sub>	0.68 <sup>+0.71</sup> <sub>-0.43</sub>	LC	
Kepler-783b	1.939 <sup>+0.165</sup> <sub>-0.142</sub>	CKS+Gaia	4.293	1.64	12.36 <sup>+0.34</sup> <sub>-0.30</sub>	88.47 <sup>+0.98</sup> <sub>-0.81</sub>	1.26 <sup>+1.39</sup> <sub>-0.88</sub>	LC	
Kepler-219b	0.840 <sup>+0.075</sup> <sub>-0.069</sub>	CKS+Gaia	4.585	4.95	9.84 <sup>+0.28</sup> <sub>-0.27</sub>	87.46 <sup>+0.48</sup> <sub>-0.37</sub>	1.85 <sup>+0.36</sup> <sub>-0.43</sub>	SC	b
Kepler-356b	0.562 <sup>+0.049</sup> <sub>-0.046</sub>	KIC+Gaia	4.613	2.84	8.59 <sup>+0.25</sup> <sub>-0.22</sub>	85.50 <sup>+0.34</sup> <sub>-0.29</sub>	1.80 <sup>+0.30</sup> <sub>-0.32</sub>	LC	
Kepler-1365c	0.360 <sup>+0.032</sup> <sub>-0.027</sub>	CKS+Gaia	4.775	1.61	7.57 <sup>+0.21</sup> <sub>-0.21</sub>	85.32 <sup>+0.70</sup> <sub>-0.53</sub>	2.09 <sup>+1.54</sup> <sub>-0.95</sub>	LC	
Kepler-321b	1.441 <sup>+0.120</sup> <sub>-0.120</sub>	CKS+Gaia	4.915	2.66	12.30 <sup>+0.36</sup> <sub>-0.30</sub>	87.67 <sup>+0.28</sup> <sub>-0.24</sub>	0.25 <sup>+0.21</sup> <sub>-0.16</sub>	LC	b
Kepler-376b	0.500 <sup>+0.047</sup> <sub>-0.040</sub>	KIC+Gaia	4.920	2.88	8.70 <sup>+0.23</sup> <sub>-0.23</sub>	87.79 <sup>+0.99</sup> <sub>-0.70</sub>	0.80 <sup>+0.97</sup> <sub>-0.60</sub>	LC	
Kepler-634b	0.472 <sup>+0.045</sup> <sub>-0.044</sub>	KIC+Gaia	5.169	1.57	8.69 <sup>+0.17</sup> <sub>-0.20</sub>	88.93 <sup>+0.72</sup> <sub>-0.82</sub>	1.06 <sup>+0.96</sup> <sub>-0.69</sub>	LC	
Kepler-392b	0.881 <sup>+0.069</sup> <sub>-0.066</sub>	CKS+Gaia	5.342	1.47	10.97 <sup>+0.23</sup> <sub>-0.25</sub>	88.97 <sup>+0.72</sup> <sub>-0.76</sub>	0.78 <sup>+0.77</sup> <sub>-0.52</sub>	LC	
Kepler-526b	0.478 <sup>+0.038</sup> <sub>-0.038</sub>	CKS+Gaia	5.459	1.26	9.11 <sup>+0.24</sup> <sub>-0.24</sub>	86.89 <sup>+0.49</sup> <sub>-0.36</sub>	1.16 <sup>+1.26</sup> <sub>-0.84</sub>	LC	
Kepler-197b	0.907 <sup>+0.052</sup> <sub>-0.052</sub>	Astroseismology	5.599	1.85	11.46 <sup>+0.17</sup> <sub>-0.20</sub>	89.06 <sup>+0.59</sup> <sub>-0.52</sub>	0.42 <sup>+0.53</sup> <sub>-0.30</sub>	SC	
Kepler-197b	0.815 <sup>+0.067</sup> <sub>-0.059</sub>	CKS+Gaia	5.599	1.85	11.13 <sup>+0.29</sup> <sub>-0.24</sub>	88.57 <sup>+0.73</sup> <sub>-0.52</sub>	0.35 <sup>+0.45</sup> <sub>-0.24</sub>	SC	
Kepler-381b	0.482 <sup>+0.045</sup> <sub>-0.045</sub>	CKS+Gaia	5.629	1.47	9.31 <sup>+0.31</sup> <sub>-0.27</sub>	86.62 <sup>+0.52</sup> <sub>-0.41</sub>	2.77 <sup>+1.44</sup> <sub>-1.81</sub>	LC	
Kepler-33b	0.353 <sup>+0.031</sup> <sub>-0.027</sub>	CKS+Gaia	5.668	2.32	8.38 <sup>+0.16</sup> <sub>-0.20</sub>	88.35 <sup>+1.24</sup> <sub>-0.98</sub>	0.76 <sup>+1.02</sup> <sub>-0.53</sub>	SC	d, e, f
Kepler-116b	0.575 <sup>+0.054</sup> <sub>-0.048</sub>	CKS+Gaia	5.969	2.19	10.32 <sup>+0.29</sup> <sub>-0.29</sub>	86.63 <sup>+0.27</sup> <sub>-0.26</sub>	0.71 <sup>+1.71</sup> <sub>-0.59</sub>	SC	
Kepler-135b	0.630 <sup>+0.056</sup> <sub>-0.054</sub>	KIC+Gaia	6.003	1.91	10.68 <sup>+0.30</sup> <sub>-0.29</sub>	87.69 <sup>+0.71</sup> <sub>-0.46</sub>	1.01 <sup>+0.93</sup> <sub>-0.71</sub>	SC	
Kepler-132b	1.237 <sup>+0.253</sup> <sub>-0.212</sub>	CKS+Gaia	6.178	2.92	13.59 <sup>+0.72</sup> <sub>-0.62</sub>	88.49 <sup>+0.88</sup> <sub>-0.59</sub>	0.69 <sup>+0.69</sup> <sub>-0.51</sub>	LC	d
Kepler-1581b	0.572 <sup>+0.047</sup> <sub>-0.045</sub>	KIC+Gaia	6.284	1.45	10.63 <sup>+0.28</sup> <sub>-0.25</sub>	87.99 <sup>+1.00</sup> <sub>-0.68</sub>	0.88 <sup>+0.96</sup> <sub>-0.60</sub>	LC	
Kepler-335b	0.281 <sup>+0.024</sup> <sub>-0.022</sub>	CKS+Gaia	6.562	10.34	8.61 <sup>+0.21</sup> <sub>-0.21</sub>	84.97 <sup>+0.28</sup> <sub>-0.23</sub>	4.54 <sup>+0.34</sup> <sub>-0.31</sub>	LC	c
Kepler-431b	0.410 <sup>+0.032</sup> <sub>-0.028</sub>	CKS+Gaia	6.802	1.28	10.02 <sup>+0.24</sup> <sub>-0.21</sub>	87.41 <sup>+0.84</sup> <sub>-0.59</sub>	0.90 <sup>+1.13</sup> <sub>-0.65</sub>	LC	
Kepler-100b	0.454 <sup>+0.004</sup> <sub>-0.006</sub>	Astroseismology	6.887	1.86	10.43 <sup>+0.04</sup> <sub>-0.04</sub>	87.32 <sup>+0.06</sup> <sub>-0.06</sub>	1.39 <sup>+0.54</sup> <sub>-0.38</sub>	SC	c
Kepler-100b	0.428 <sup>+0.033</sup> <sub>-0.027</sub>	CKS+Gaia	6.887	1.86	10.24 <sup>+0.23</sup> <sub>-0.19</sub>	87.12 <sup>+0.26</sup> <sub>-0.21</sub>	1.66 <sup>+0.46</sup> <sub>-0.36</sub>	SC	c
Kepler-403b	0.317 <sup>+0.025</sup> <sub>-0.022</sub>	CKS+Gaia	7.031	1.94	9.25 <sup>+0.17</sup> <sub>-0.17</sub>	89.22 <sup>+0.58</sup> <sub>-0.70</sub>	0.56 <sup>+0.63</sup> <sub>-0.40</sub>	LC	
Kepler-60b	0.491 <sup>+0.044</sup> <sub>-0.040</sub>	CKS+Gaia	7.133	1.25	11.00 <sup>+0.30</sup> <sub>-0.29</sub>	88.15 <sup>+1.06</sup> <sub>-0.66</sub>	0.73 <sup>+1.08</sup> <sub>-0.53</sub>	LC	b, c, d
Kepler-853b	0.540 <sup>+0.045</sup> <sub>-0.043</sub>	CKS+Gaia	7.169	7.58	11.38 <sup>+0.29</sup> <sub>-0.30</sub>	88.43 <sup>+0.82</sup> <sub>-0.58</sub>	1.08 <sup>+0.66</sup> <sub>-0.72</sub>	LC	

Table 1 continued

Table 1 (*continued*)

Planet	$\rho_*$ (g cm <sup>-3</sup> )	Source	$P_1$ (days)	$P_2/P_1$	$a/R_*$	$i(^{\circ})$	$\Delta I(^{\circ})$	Cadence	TTV
Kepler-450d	$0.478^{+0.064}_{-0.064}$	Astreoseismology	7.514	2.05	$11.29^{+0.32}_{-0.30}$	$88.55^{+0.73}_{-0.50}$	$0.39^{+0.40}_{-0.26}$	SC	b, c
Kepler-450d	$0.438^{+0.029}_{-0.028}$	CKS+Gaia	7.514	2.05	$11.06^{+0.20}_{-0.18}$	$88.16^{+0.37}_{-0.29}$	$0.99^{+0.38}_{-0.40}$	SC	b, c
Kepler-216b	$0.425^{+0.038}_{-0.034}$	CKS+Gaia	7.694	2.26	$11.09^{+0.28}_{-0.30}$	$88.68^{+0.71}_{-0.54}$	$0.65^{+0.59}_{-0.47}$	SC	
Kepler-200b	$1.300^{+0.124}_{-0.109}$	CKS+Gaia	8.595	1.19	$17.19^{+0.53}_{-0.52}$	$88.34^{+0.39}_{-0.30}$	$0.84^{+0.56}_{-0.41}$	LC	
Kepler-338e	$0.309^{+0.034}_{-0.034}$	Astreoseismology	9.342	1.47	$11.28^{+0.31}_{-0.36}$	$88.50^{+0.69}_{-0.52}$	$0.74^{+0.68}_{-0.49}$	SC	
Kepler-338e	$0.293^{+0.024}_{-0.022}$	CKS+Gaia	9.342	1.47	$11.07^{+0.29}_{-0.23}$	$88.20^{+0.53}_{-0.37}$	$1.00^{+0.58}_{-0.66}$	SC	
Kepler-804c	$1.168^{+0.109}_{-0.098}$	CKS+Gaia	9.652	1.49	$17.67^{+0.42}_{-0.41}$	$89.56^{+0.32}_{-0.39}$	$0.36^{+0.40}_{-0.26}$	LC	
Kepler-36b	$0.361^{+0.024}_{-0.022}$	CKS+Gaia	13.850	1.17	$15.41^{+0.13}_{-0.19}$	$89.48^{+0.32}_{-0.30}$	$0.29^{+0.28}_{-0.21}$	SC	b, c
Kepler-277b	$0.316^{+0.027}_{-0.025}$	CKS+Gaia	17.324	1.91	$15.99^{+0.13}_{-0.18}$	$89.75^{+0.17}_{-0.25}$	$1.06^{+0.64}_{-0.80}$	SC	b

<sup>a</sup>PDF of a Rayleigh distribution

**Table 2.** Model comparison with Hierarchical Bayesian Modeling

Model for $\Delta I$	Bayesian Evidence $\log(Z)$	Parameters	Prior
1: $\Delta I \sim P(\sigma_0)$ <sup>b</sup>	-41.9	$\sigma_0 = 0.0504_{-0.0025}^{+0.0024}$ (RMS $\Delta I = 4.05_{-0.20}^{+0.19}$ °)	$\sigma_0$ : log-uniform [-5,5]
2: $\Delta I \sim P(\sigma_0(\frac{a}{R_\star})^m)$	-8.3	$\sigma_0 = 0.382_{-0.063}^{+0.080}$ $m = -1.28 \pm 0.10$	$\sigma_0$ : log-uniform [-5,5] $m$ : uniform [-5,5]
3: $\Delta I \sim P(\sigma_1)$ if $\frac{a}{R_\star} < \frac{a'}{R_\star'}$ $\Delta I \sim P(\sigma_2)$ if $\frac{a}{R_\star} > \frac{a'}{R_\star'}$	-15.1	$\sigma_1 = 0.0830_{-0.0069}^{+0.0079}$ (RMS $\Delta I = 6.68_{-0.55}^{+0.64}$ °) $\sigma_2 = 0.0250_{-0.0014}^{+0.0016}$ (RMS $\Delta I = 2.01_{-0.11}^{+0.13}$ °) $\frac{a'}{R_\star'} = 4.65_{-0.10}^{+0.27}$	$\sigma_1$ : log-uniform [-5,5] $\sigma_2$ : log-uniform [-5,5] $\frac{a'}{R_\star'}$ : log-uniform [0,2]
4: $\Delta I \sim P(\sigma_1)$ if $\frac{P_2}{P_1} < \frac{P_2'}{P_1'}$ $\Delta I \sim P(\sigma_2)$ if $\frac{P_2}{P_1} > \frac{P_2'}{P_1'}$	-27.1	$\sigma_1 = 0.0311_{-0.0022}^{+0.0021}$ (RMS $\Delta I = 2.50_{-0.18}^{+0.17}$ °) $\sigma_2 = 0.0765_{-0.0066}^{+0.0081}$ (RMS $\Delta I = 6.15_{-0.53}^{+0.65}$ °) $\frac{P_2'}{P_1'} = 5.38_{-0.86}^{+0.56}$	$\sigma_1$ : log-uniform [-5,5] $\sigma_2$ : log-uniform [-5,5] $\frac{P_2'}{P_1'}$ : log-uniform [0,2]

<sup>b</sup>PDF of a Rayleigh distribution